Fatigue life prediction for Waspaloy under biaxial loading☆

J.V. Sahadi[a,*], D. Nowell[a], R.J.H. Paynter[a]

[a]*Department of Engineering Science, University of Oxford, Parks Road, Oxford OX1 3PJ, UK*

Abstract

This investigation revisits biaxial fatigue experiments carried out with nickel-based superalloy Waspaloy. Recently, yield criteria extended to multiaxial fatigue and stress-based approaches have been analysed, and their performances in correlating biaxial test data have been evaluated. It has been concluded that despite giving reasonable results, the parameters do not properly represent the physical behaviour of the material. An extension of the study is therefore executed using the strain based critical plane approaches proposed by Wang-Brown and Fatemi-Socie, and the energy-based approaches proposed by Smith-Watson-Topper, Liu and Ince-Glinka. Reasonably good fatigue life predictions are obtained with all criteria. However, for low cycle fatigue regime, best correlation is obtained with the Liu parameter.

Keywords: Biaxial fatigue, Fatigue Life, Waspaloy, Critical Plane Approach
2018 MSC: 00-00, 00-00

1. Introduction

The safety and reliability of complex systems, such as nuclear reactors, gas turbines and aircrafts, are strongly correlated to the design of the constituent parts and to the dynamic forces acting during their operation. Cyclic loading, even for stress levels considerably below the ultimate strength of the material, facilitates movement of dislocations, which eventually form persistent slip bands at critical points. Some of these slip bands grow to form extrusions and/or intrusions that may lead to the nucleation of micro-cracks. Finally, one of the micro-cracks dominates the fatigue process by propagating and leading to final failure [1, 2].

Often, mechanical components are designed considering ideal uniaxial loading conditions, due to the simplicity and cost effectiveness of uniaxial testing and the amount of experimental data available. However, engineering components and structures are commonly loaded by a combination of variable loads in multiple directions, due to their complex geometry and/or complexity of external loading. In contrast to uniaxial fatigue, the multiaxial fatigue problem involves complex stress/strain states, mean stress effects, loading history dependency and non-proportional hardening. Thus, the study of multiaxial fatigue requires experiments to properly reproduce such loading conditions and fatigue damage parameters which accurately predict multiaxial fatigue lives.

There exist numerous standards and preferred methods for fatigue testing and specimen geometries. For instance, tension-torsion tests with thin-walled tubular specimens are commonly used to investigate multiaxiality effects. However, although numerous different approaches have been proposed for modelling, there is no universal consensus on the most efficient criterion for predicting multiaxial fatigue failure. Most of the criteria proposed are limited to certain materials and/or specific loading conditions.

In this regard, the present paper further investigates biaxial fatigue tests carried out at the University of Oxford with cruciform specimens made of the nickel-based superalloy Waspaloy. In the initial study [3], a combination of stress-based formulations was investigated, including yield criteria extended to multiaxial fatigue, invariant-based formulations and critical plane approaches. Despite the reasonably good agreement between experimental fatigue life and predicted life, none of the formulations assessed correctly captured the physical behaviour of the material (e.g. by predicting the correct initiation angle). Hence, we propose here to extend the initial investigation by assessing a number of strain- and energy-based formulations.

☆Manuscript for Special Issue of Theoretical and Applied Fracture Mechanics.

*Corresponding author
Email address: joao.sahadicavalheiro@eng.ox.ac.uk (J.V. Sahadi)

1.1. Multiaxial Fatigue Testing

Lanza [4] pioneered multiaxial fatigue experiments by observing combined cyclic loading back in 1886. He discussed his test results for combined in-phase bending and torsion and pointed out the need for further work. Later, Mason [5] conducted an extensive study of cyclic strains under combined fully reversed torsional and bending stresses on mild steel. At the time, multiaxial fatigue was still in its infancy and the term itself had not yet been coined.

A significant contribution was made by Manson and co-workers in the early 1920s. Their work, [6] published in 1923, is considered the pioneer in detailed elastic-plastic analysis in the high cycle fatigue regime. They use a bilinear representation for the cyclic stress-strain curve in the case of round bars under alternating torsion or bending [7]. In addition, Manson and Delaney [8] published the first report on out-of-phase combined bending and torsion.

A more systematic multiaxial fatigue test programme was conducted in the 1930s by Gough and Pollard [9], who designed and built high speed testing machines to investigate the combined effects of bending and torsional stresses (with and without mean stresses) on fatigue life. This set of experiments was used as a benchmark for the early multiaxial fatigue criteria, such as the empirical proposition of Gough [10] (for ductile steels and cast-irons) and the first stress-based multiaxial criteria. Yet another extensive investigation of fatigue strength under combined bending and torsion was published by Nishihara and Kawamoto [11–13]. Their experimental data has been widely used for benchmarking.

Advances in material testing equipment and techniques during the past 40 years have enabled the development of more realistic multiaxial fatigue tests by applying loads representative of service life, at different temperatures, test frequencies and load phase difference. Among the most used techniques, cruciform specimens and thin-walled tubular specimens have been broadly used for fatigue testing under biaxial stress states [14]. However, tension-torsion specimens pose limitations for probing the entire principal stress plane, σ_1 vs σ_2, since only 2 of the 4 quadrants can be investigated. Nevertheless, using internally-pressurized tubular specimens, it is possible to access more of the principal stress plane.

Figure 1 illustrates the regions of the principal stress plane, σ_1 vs σ_2, that can be probed depending on the test configuration. The combination of cruciform specimens and axial-torsional specimens, internally pressurized, allows the investigation of almost the entire principal stress plane. However, for cruciform specimens the assessment of the biaxial compression region is challenging due to potential specimen buckling limitations. In the literature, examples of fatigue life investigation using tubular specimens are available in [15–17]. Cruciform specimens and biaxial test rigs allow the investigation of a broad range of biaxiality. However, specimens are expensive, and testing is complex [18–20].

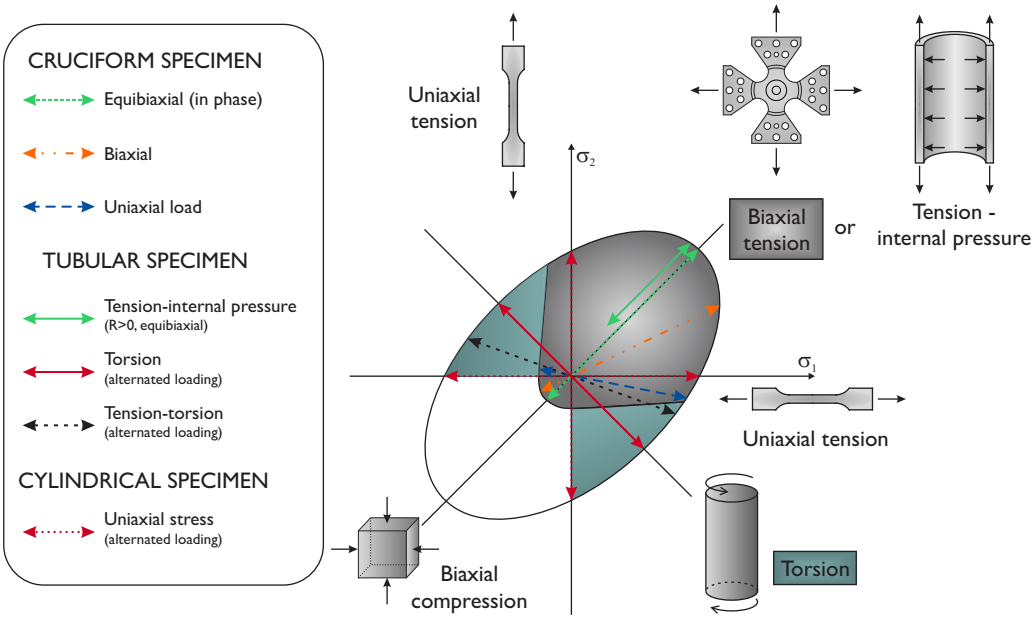

Figure 1: Possible stress domain and corresponding experiments. Adapted from [14].

2. Material and Methods

Our earlier work on multiaxial fatigue has presented biaxial tests on Waspaloy [3], a nickel-based superalloy widely used for disks in aero-engines. This material presents elevated creep resistance, high fatigue strength, low thermal expansion coefficient and high thermal conductivity; essential characteristics to sustain the extreme mechanical and thermal loads to which aero-engine disks are subjected.

Load controlled tests were carried out at a load ratio of $R = 0.05$ and 0.5Hz frequency using a biaxial servo-hydraulic rig, developed and built at the University of Oxford. The rig consists of two independent frames carrying hydraulic actuators, such that the perpendicular load vectors meet at the centre of the specimen. The vertical load path has a fixed clamp at the top and an actuator at the bottom capable of providing up to 350kN. The horizontal load path has two actuators, providing up to 100kN each. The two frames are connected to each other through a set of springs, which allow vertical movement of the horizontal actuators as the specimen deforms.

All tests were performed using a cruciform specimen with reduced thickness gauge section at the centre (Figure 2). The centre portion (excluding the gauge section) was shot peened to increase the fatigue strength of the external edges between the arms and hence to inhibit failure away from the gauge section. Strain gauge rosettes were mounted on both front and back face of the gauge section and at the narrow point of the arms. The outputs from these were recorded, together with the applied loads, to determine the calibration of the specimen.

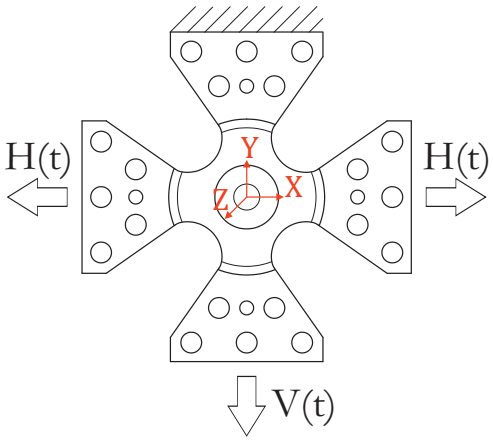

Figure 2: Cruciform specimen, applied loads and definition of $x - y - z$ coordinate system.

In terms of its mechanical properties, the axial hardening curve for Waspaloy at room temperature was obtained from Pattison [21], who used deformation-controlled tests with thin-walled tubular specimens. The material has a Poisson's ratio of $\nu = 0.284$ and Young's modulus of $E = 222$ GPa. Figure 3 presents the axial monotonic and cyclic stress-strain response of the material. The cyclic hardening curve was modelled using the Ramberg-Osgood power law for cyclic loading to fit the stabilised plastic strain and stress amplitude test data, as is defined in:

$$\frac{\Delta\varepsilon}{2} = \frac{\Delta\sigma}{2E} + \left(\frac{\Delta\sigma}{2K'}\right)^{\frac{1}{n'}} \quad , \tag{1}$$

where K' and n' are the axial fatigue strength coefficient and the cyclic axial strain hardening exponent, respectively. These parameters can be obtained by fitting true stress versus plastic strain in a log-log scale [22].

2.1. Load Combination

The original load conditions were set to have the same maximum principal stress in each case, varying the other in-plane principal stress. As the gauge section is only 2mm thick and 15mm across, the assumption is made that the local behaviour is equivalent to plane stress conditions, i.e. that the stress in the through thickness direction is zero. The following combinations were investigated:

- Equal biaxial tension (EB): Equal load applied to each arm ($\sigma_1 = \sigma_2$);
- Pure shear (PS): Stresses on the two axes are equal and opposite ($\sigma_1 = -\sigma_2$);

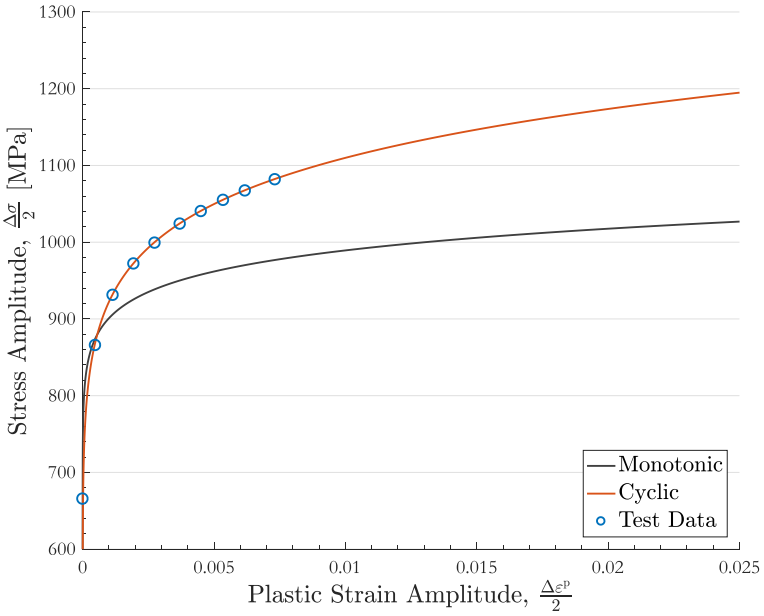

Figure 3: Cyclic hardening curve for Waspaloy at room temperature. Adapted from [21].

– Single Actuator (Uniaxial Load UL): Load applied on one axis only;

– Uniaxial Stress (US): Both axes are used to create an uniaxial equivalent stress state at the gauge section ($\sigma_2 = 0$);

– Minimum von Mises (Mv): The combination of loads that gives the minimum von Mises equivalent stress (octahedral shear stress) at the gauge section, i.e. for a given σ_1, σ_2 is calculated to give the minimum von Mises equivalent stress under biaxial tension.

2.2. Experimental Results

As is presented in more detail in Sahadi et al [3], the initial tests compared different biaxialities at the same $\sigma_{1,\text{peak}}$, but different $\sigma_{2,\text{peak}}$ for each test. Further tests for the pure shear and uniaxial stress cases were run at lower peak stresses. It was observed that in most cases yielding occurred during the first cycle, but no "reversed yielding" took place when load was removed. Hence subsequent load cycles at the same load level were essentially elastic. This observation is important as it sets the context for the multiaxial criteria which are appropriate.

To translate between the loads applied by the actuators and the stress at the gauge section an elastic relationship was established. The data for this was obtained from measurements during the elastic loading phase of testing. The normalised compliance response found for the rosette located at the centre of the gauge section is $c_p = 0.0117\mu\varepsilon/\text{kN}$ for the axis parallel to loading and $c_n = -0.0063\mu\varepsilon/\text{kN}$ for the normal direction (the ratio $r_\varepsilon = c_n/c_p = -0.538$). Hence, for any combination of loads the normalised nominal strains can be calculated by:

$$\varepsilon_x = 0.0117L_H - 0.0063L_V \quad , \tag{2}$$

and

$$\varepsilon_y = -0.0063L_H + 0.0117L_V \quad , \tag{3}$$

where L_H and L_V are the horizontal and vertical nominal loads, respectively.

Assuming a plane stress state at the gauge section, the nominal stress state at the centre of the specimen can be calculated by:

$$\sigma_x = \frac{E}{1-\nu^2}\left(\varepsilon_x + \nu\varepsilon_y\right) \quad , \tag{4}$$

and

$$\sigma_y = \frac{E}{1-\nu^2}\left(\varepsilon_y + \nu\varepsilon_x\right) \quad , \tag{5}$$

Nominal stress and strain levels were used to set the experimental conditions (estimate the loads required for each test), and actual strain gauge readings were used to confirm whether the required values were achieved.

Table 1 summarizes the results obtained after testing of 11 specimens. Note that stress and strain levels presented in Tab. 1 are nominal, calculated using Eqs. 2–5. The map of peak stresses in the two principal directions (σ_1 *vs* σ_2) shown in Fig 4 graphically represents the test cases shown in Tab. 1. It gives a diagrammatical summary of the load conditions, with life to failure ('000 cycles) shown below each case point. von Mises and elastic strain energy contours were plotted in Figure 4 as guides to represent the initial elastic domain of Waspaloy.

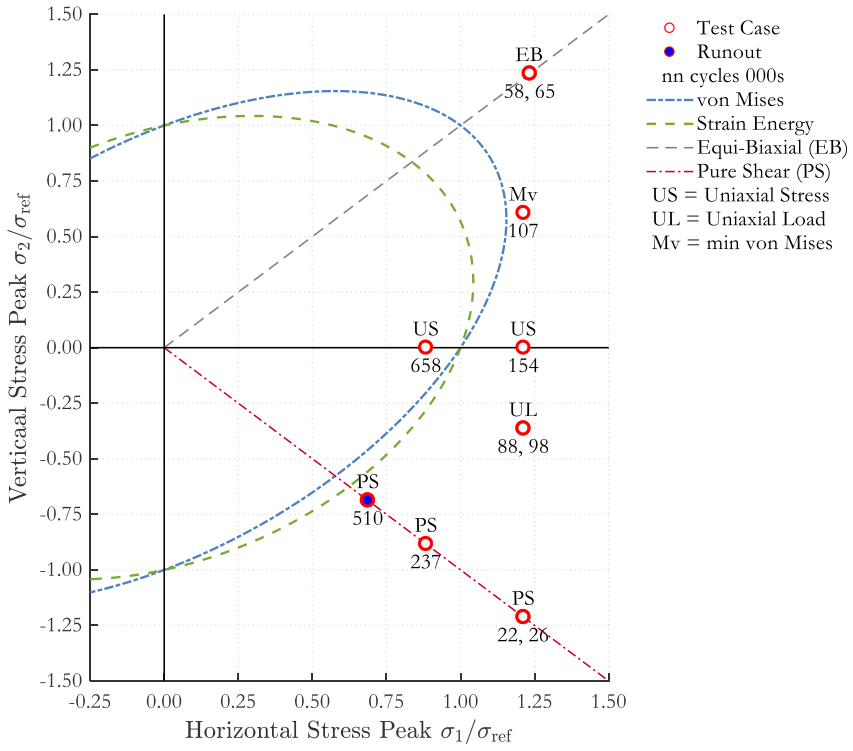

Figure 4: Map of Stress Concentration for $\sigma_3 = 0$. Each point represents a test case. The resulting life is shown in thousands of cycles below each point. For cases with two test results, both values are given.

Table 1: Experimental tests parameters and results – nominal stress and strain values.

Exp. №	Load Case	Peak Load [kN]		Norm. Peak Strain		Norm. Peak Stress			Biaxiality Ratio			Cycles, $2N_f$
		Horizontal	Vertical	ε_x	ε_y	σ_x	σ_y	σ_{vM}	Load	Strain	Stress	
CX01	Equi-Biaxial	127	0	1.489	-0.801	1.372	-0.412	1.618	0.00	-0.54	-0.30	87,765
CX02	Equi-Biaxial	170	170	0.921	0.921	1.286	1.286	1.286	1.00	1.00	1.00	65,426
CX03	Equi-Biaxial	170	170	0.921	0.921	1.286	1.286	1.286	1.00	1.00	1.00	57,884
CX04	Single Actuator	117	0	1.372	-0.738	1.264	-0.379	1.490	0.00	-0.54	-0.30	97,560
CX05	Pure Shear	90	-90	1.623	-1.623	1.264	-1.264	2.189	-1.00	-1.00	-1.00	25,789
CX06	Pure Shear	51	-51	0.920	-0.920	0.716	-0.716	1.241	-1.00	-1.00	-1.00	510,000[a]
CX07	Uniax Equiv	129	39	1.264	-0.359	1.264	0.000	1.264	0.30	-0.28	0.00	154,396
CX08	Min von Mises	148	103	1.084	0.273	1.264	0.632	1.095	0.70	0.25	0.50	107,004
CX09	Uniax Equiv	94	28	0.920	-0.261	0.920	0.000	0.920	0.30	-0.28	0.00	658,164
CX10	Pure Shear	66	-66	1.182	-1.182	0.920	-0.920	1.594	-1.00	-1.00	-1.00	236,935
CX11	Pure Shear	90	-90	1.623	-1.623	1.264	-1.264	2.189	-1.00	-1.00	-1.00	21,684

[a] Runout

2.3. Stress and Strain Ranges

Finite Element modelling was used to obtain the actual stress ranges for each loading condition, as the relationship between load and stress/strain is not obvious for the cruciform specimen. Due to the symmetry of the problem, only one eighth of the specimen was modelled with appropriate boundary

conditions imposed to the symmetry planes. Under applied cyclic loading, stress-strain responses at the gauge section showed a transient response, but stabilized over a number of loading cycles. All test conditions were performed under proportional load. Therefore, the FE model was provided with the stabilized cyclic stress-stress response, described in Figure 3.

All the strain- and energy-based formulations presented in the following section follow the critical-plane approach. Therefore, the elastic and plastic strain components for the critical plane search algorithm were calculated considering Hooke's law and Hencky's total deformation plasticity equation [23]:

$$\varepsilon_{ij} = \frac{1+\nu}{E}\sigma_{ij} - \frac{\nu}{E}\sigma_{kk}\delta_{ij} + \frac{3}{2}\frac{\varepsilon^p_{eq}}{\sigma_{eq}}S_{ij} \quad , \tag{6}$$

where ε_{ij} represents the total strain components, σ_{ij} the stress components of Cauchy's stress tensor and S_{ij} the deviatoric stress components, given by:

$$S_{ij} = \sigma_{ij} - \frac{1}{3}\sigma_{kk}\delta_{ij} \quad . \tag{7}$$

The remaining terms, σ_{eq} and ε^p_{eq}, are the von Mises equivalent stress and equivalent plastic strain, respectively:

$$\sigma_{eq} = \sqrt{\frac{3}{2}S_{ij}S_{ij}} \quad , \tag{8}$$

$$\varepsilon^p_{eq} = \sqrt{\frac{2}{3}\varepsilon^p_{ij}\varepsilon^p_{ij}} \quad . \tag{9}$$

The relationship between these, for the multiaxial stress state, is the Ramberg-Osgood power law presented in Eq. 1:

$$\varepsilon^p_{eq} = \left(\frac{\sigma_{eq}}{K'}\right)^{\frac{1}{n'}} \quad , \tag{10}$$

Table 2 presents the actual stress and strain ranges seen during the tests. i.e. it presents the average strain amplitude and average mean strain measured with strain gauge rosettes and the actual residual and peak stresses obtained with an elastic-plastic Finite Element analysis, considering the peak loads measured by the load cells of the biaxial rig. Critical residual and peak stresses for each test condition were obtained from the points of maximum von Mises equivalent stress in the gauge section.

Table 2: Experimental tests parameters and results based on strain gauge readings and FE analysis.

Exp. №	Load Case	Peak Load [kN]		Mean Strain			Strain Amplitude			Residual Stress		Peak Stress		Cycles, $2N_f$
		Horizontal	Vertical	ε_x	ε_y	ε_{xy}	ε_x	ε_y	ε_{xy}	σ_x	σ_y	σ_x	σ_y	
CX01	Single Actuator	126.33	8.07	1.396	-0.469	0.359	0.690	-0.367	0.132	-0.19	0.07	1.12	-0.23	87765
CX02	Equi-Biaxial	169.34	172.67	1.049	1.098	1.075	0.445	0.436	0.436	-0.04	-0.04	1.18	1.23	65426
CX03	Equi-Biaxial	170.73	170.98	1.180	1.143	1.141	0.450	0.452	0.459	-0.04	-0.04	1.20	1.21	57884
CX04	Single Actuator	118.20	1.15	1.154	-0.676	0.199	0.662	-0.358	0.145	-0.17	0.07	1.08	-0.28	97560
CX05	Pure Shear	92.32	-90.40	1.209	-1.121	0.241	0.327	-0.326	0.072	-0.42	0.42	0.80	-0.80	25789
CX06	Pure Shear Low	52.15	-51.22	0.638	-0.622	0.014	0.444	-0.440	0.014	-0.04	0.04	0.66	-0.66	510000[a]
CX07	Uniax Equiv	130.30	38.70	0.852	-0.301	0.261	0.612	-0.178	0.198	-0.08	0.02	1.19	0.01	154396
CX08	Min von Mises	150.25	103.22	0.645	0.134	0.343	0.525	0.127	0.313	0.00	0.00	1.29	0.57	107004
CX09	Uniax Equiv Low	96.41	28.33	0.502	-0.145	0.121	0.452	-0.133	0.144	0.03	0.00	0.97	-0.01	658164
CX10	Pure Shear	67.74	-65.88	1.093	-1.035	0.069	0.584	-0.574	0.017	-0.16	0.16	0.74	-0.73	236935
CX11	Pure Shear	93.00	-90.40	1.581	-1.365	0.170	0.342	-0.327	0.018	-0.42	0.42	0.81	-0.80	21684

[a] Runout

Both tables (Tabs.1 and 2) present similar stress ranges. However the results obtained with the elastic-plastic FE analysis show that there was a significant level of residual stresses for the single actuator (CX01 and CX04) and pure shear (CX05, CX10 and CX11) test cases. Therefore, for these test cases the actual peak stresses are considerably different than the nominal ones.

3. Multiaxial Fatigue Modelling

The fatigue behaviour of materials is characterized in the form of a stress or strain parameter versus fatigue life, and a cyclic stress-strain curve. Such a characterization is usually obtained using smooth specimens under uniaxial loading. Multiaxial fatigue assessment is then carried out with the help of

an appropriate rule or criterion that reduces the complex multiaxial stress/strain state to an equivalent uniaxial stress/strain state. For high cycle fatigue regime, fatigue life is commonly estimated using a combination of stress-based theories and the relationship established by Basquin. For axial loading, this relationship is given by:

$$\frac{\Delta\sigma}{2} = \sigma'_f (2N_f)^b \quad , \tag{11}$$

and for torsional/shear loading:

$$\frac{\Delta\tau}{2} = \tau'_f (2N_f)^{b_\gamma} \quad . \tag{12}$$

In terms of elastic axial and shear strain, Eqs. 11 and 12 can be rewritten as follows:

$$\frac{\Delta\varepsilon^e}{2} = \frac{\sigma'_f}{E} (2N_f)^b \quad , \tag{13}$$

and,

$$\frac{\Delta\gamma^e}{2} = \frac{\tau'_f}{G} (2N_f)^{b_\gamma} \quad , \tag{14}$$

where $\Delta\sigma$ and $\Delta\tau$ are the axial and shear stress ranges, and $\Delta\varepsilon^e$ and $\Delta\gamma^e$ the axial and shear elastic strain ranges, respectively. σ'_f and b are the axial fatigue strength coefficient and exponent, respectively. Analogously, τ'_f and b_γ are the shear fatigue strength coefficient and exponent, respectively. N_f is the number of reversals ($2N_f$ refers to the number of cycles to failure).

However, many components and structures undergo a few cycles of high amplitude stress during their lifetime (i.e. take-off and landing of aircrafts, start-up and shut-down of power generation plants, etc.). Design for this life region (life $< 10^5$ cycles) is referred to as low cycle fatigue design for which localized cyclic plasticity plays an important role. For the past 60 years, cyclic strain has been the basis for low cycle fatigue design. Hence, predictions for low cycle fatigue regime are made by the association of strain-based criteria with the following strain-life relationship for axial loading:

$$\frac{\Delta\varepsilon}{2} = \frac{\Delta\varepsilon^e}{2} + \frac{\Delta\varepsilon^p}{2} = \frac{\sigma'_f}{E} (2N_f)^b + \varepsilon'_f (2N_f)^c, \tag{15}$$

where $\Delta\varepsilon$ is the total axial strain range, and equal the sum of elastic and plastic strain ranges. ε'_f and c are the axial fatigue ductility coefficient and exponent, respectively. Similarly, for torsional/shear loading:

$$\frac{\Delta\gamma}{2} = \frac{\Delta\gamma^e}{2} + \frac{\Delta\gamma^p}{2} = \frac{\tau'_f}{G} (2N_f)^{b_\gamma} + \gamma'_f (2N_f)^{c_\gamma}, \tag{16}$$

where $\Delta\gamma$ is the total shear strain range, and equal the sum of elastic and plastic strain ranges. γ'_f and c_γ are the shear fatigue ductility coefficient and exponent, respectively. Eqs. 15 and 16 are a combination of Basquin's and Coffin-Manson's relationships.

The following sections present some of the most widely used multiaxial fatigue theories. Of course, it is not possible to review all the models that have been proposed in the literature. For a chronological review of multiaxial fatigue criteria see [7, 24–26]. For a more detailed review of stress-, strain- and energy-based multiaxial criteria refer to [25–30]. Critical plane approaches have also been assessed in [30–33]; Finally, for a consistent experimental data base see: [34].

The theories described in here are presented in three main different classes, stress-based, strain-based and energy-based criteria. These approaches are classified based on the parameter used to quantify fatigue damage.

3.1. Stress-based criteria

An introductory analysis of the test data was achieved by considering extensions of yield theories to multiaxial fatigue and stress-based criteria. The formulations of von Mises, elastic strain energy equivalent stress, Crossland [35], Findley [36] and Matake [37] were investigated. Among them, the energy parameter and Crossland's invariant based approach gave the best predictions.

The elastic strain energy density is the sum of the products of strain and stress (divided by 2). In the case of plane stress and no shear, a uniaxial stress with strain energy equivalent to a biaxial stress state is formulated as follows:

$$\sigma_{\mathrm{Ue}} = \sqrt{\sigma_1^2 + \sigma_1^2 - 2\nu\sigma_1\sigma_2} \quad , \tag{17}$$

Figure 5 presents the correlation between this parameter normalised and the test data in cycles to failure, considering the nominal stress values presented in Tab. 1. The stress-life curve was obtained

using Basquin's relation for stress (Eq. 11) and using the equivalent stress presented in Eq. 17. The criterion provided good results with a correlation coefficient, R^2, of 0.868. Among all the test cases, the pure shear case (CX10) was the furthest from the line of best-fit.

Analogously, Figure 6 presents the results obtained with the elastic strain energy parameter and the actual stress levels from Tab. 2. In order to reduce scatter and account for mean stress effects, the energy parameter was associated with the Walker stress criterion [38], and formulated as:

$$\sigma_{\mathrm{W}} = \left(\sigma_{\mathrm{Ue,peak}}\right)^{1-m} \left(\sigma_{\mathrm{Ue,a}}\right)^{m} \quad , \tag{18}$$

where $\sigma_{\mathrm{Ue,peak}}$ and $\sigma_{\mathrm{Ue,a}}$ are the peak and amplitude of the elastic strain energy equivalent stress, respectively. σ_W represents the Walker stress and m the Walker exponent, a fitting parameter used to collapse both mean stress and multi-axial effects. The exponent in this correlation was optimised to $m = 0.645$, improving correlation with the experimental data, $R^2 = 0.9107$, and reducing the scatter observed with the pure shear case (CX10).

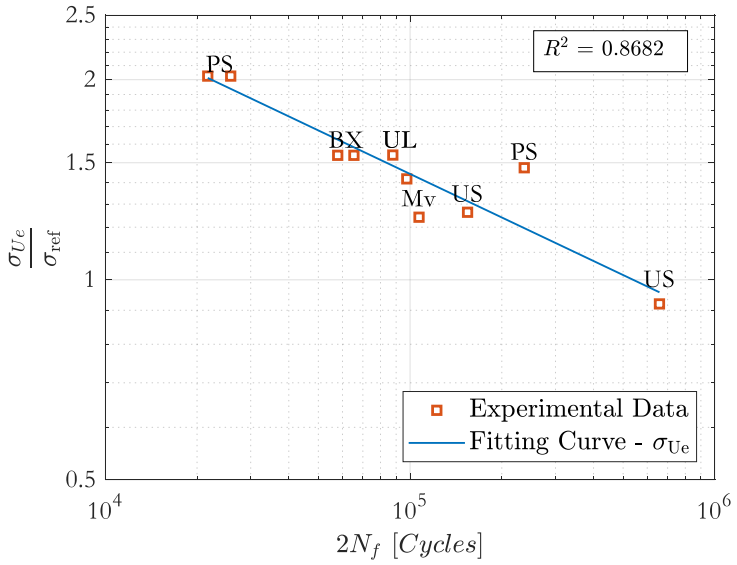

Figure 5: Fatigue life prediction with elastic strain energy density – Nominal stress values.

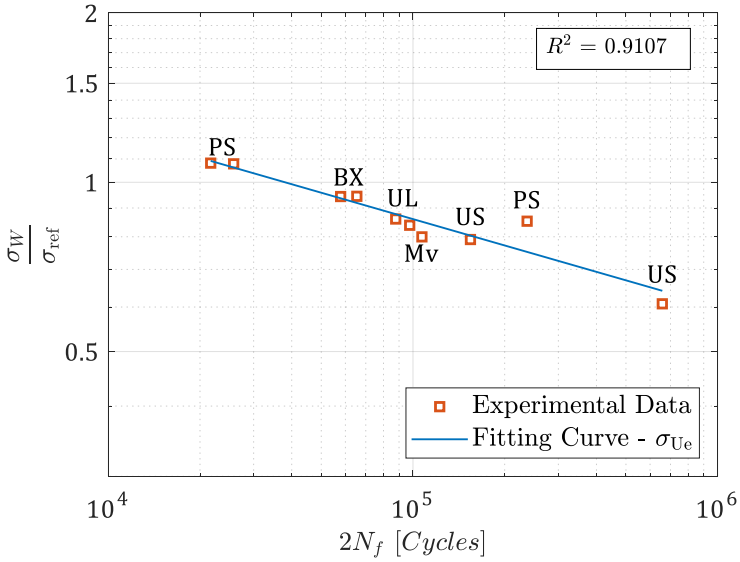

Figure 6: Fatigue life prediction with elastic strain energy density – Actual stress values from FE analysis.

Next, some of the most widely used stress-based criteria were investigated. The stress invariant based criterion proposed by Crossland [35] considers the amplitude of the second invariant of the deviatoric stress tensor, J_{2a} (which corresponds to the amplitude of von Mises equivalent stress) and the maximum value of the first invariant of Cauchy's stress tensor, i.e. the maximum hydrostatic stress, $\sigma_{\mathrm{h,max}}$. This last term accounts for the mean stress effect. The criterion is given as:

$$\sqrt{J_{2a}} + \kappa \sigma_{h,\max} = \lambda \quad , \tag{19}$$

where κ and λ are material constants determined under fully reversed tension (σ_{-1}) and torsion (τ_{-1}) tests with smooth specimens respectively:

$$\kappa = 3\left(\frac{\tau_{-1}}{\sigma_{-1}}\right) - \sqrt{3} \quad ; \quad \lambda = \tau_{-1} \quad . \tag{20}$$

Figure 7 presents the fatigue life predictions obtained with this formulation, considering various fatigue thresholds, i.e. a test case below a line is predicted to have a longer fatigue life than the threshold of the line. On the other hand, a point above it represents a test case with shorter life. The light grey shade area corresponds to the calibrated region (tension-torsion), and is delimited by the uniaxial tension dashed lines. The darker grey shade area is delimited by the equi-biaxial line. The dashed black lines connect test cases with the same $\sigma_{1,\mathrm{peak}}$, in order to illustrate the biaxiality effect when $\sigma_{2,\mathrm{peak}}$ is changed.

It is concluded that in general the model presents good correlation with experimental data both within and outside the tension-torsion calibration region. However, non-conservative predictions are obtained for negative values of $\sigma_{2,\mathrm{peak}}$ (pure shear and uniaxial load cases – CX01, CX04, CX05 and CX10). In contrast, as $\sigma_{2,\mathrm{peak}}$ increases towards higher positive values, the criterion becomes proportionally more conservative (minimun von Mises and equi-biaxial – CX08, CX02 and CX03).

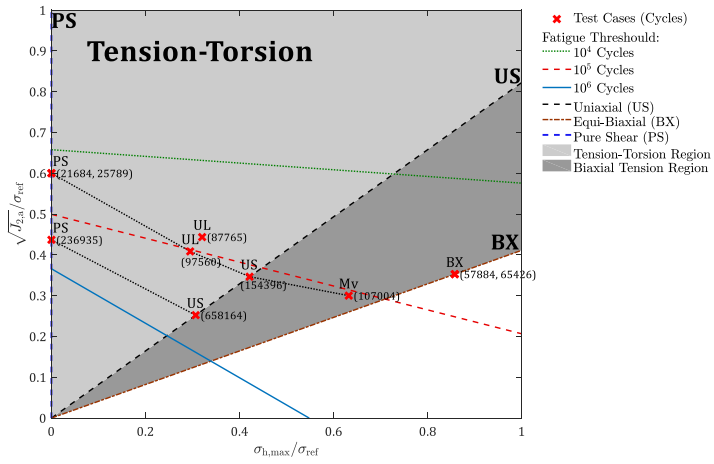

Figure 7: Fatigue life predictions according to Crossland's criterion.

3.2. Strain-based criteria

Despite the satisfactory results obtained with the stress-based criteria, it was concluded in the previous investigation that they do not properly represent the physical behaviour of materials. In this context, a further analysis is performed using strain-based critical plane approaches. This class of strain-based methods determines critical planes (one or more) where a particular damage parameter reaches its maximum magnitude. This methodology has gained great attention over the past 40 years as it mathematically describes the physical phenomenon and is capable of predicting damage and also the crack orientation (for ductile materials, cracks typically nucleate along slip planes, where the maximum shear stress occurs [28, 39]). Two of the most widely used criteria: the Fatemi-Socie [40] and Wang-Brown [41] parameters are evaluated here.

Brown and Miller [39] proposed a theory based on a physical interpretation of mechanisms of fatigue crack growth. According to them, failure under multiaxial fatigue is governed by the maximum shear stress range. In addition, the tensile normal strain acting on the plane of maximum shear strain benefits propagation (by opening the crack tip). Originally, Brown and Miller represented graphically their

criterion by contours of constant life. Later Kandil, Brown and Miller [42] proposed a specific formulation of the theory for 'Case A' cracks, which propagate along the surface:

$$\Delta\hat{\gamma} = (\Delta\gamma_{\max}^{\alpha} + S\Delta\varepsilon_{\mathrm{n}}^{\alpha})^{\frac{1}{\alpha}} \quad , \tag{21}$$

where $\Delta\hat{\gamma}$ is the equivalent shear strain range, $\Delta\gamma_{\max}$ is taken as the maximum shear strain range and $\Delta\varepsilon_{\mathrm{n}}$ is the normal strain range on the plane of maximum shear strain range. S represents a material dependent parameter, describing the influence of the normal strain on material crack growth. Similar to the material constants for Crossland's formulations, S is also determined by correlating axial and torsional fatigue data.

Finally, Wang-Brown [41] introduced a mean stress term to the formulation, and assuming $\alpha = 1$, the equivalent shear strain amplitude was expressed as:

$$\frac{\Delta\hat{\gamma}}{2} = \frac{\Delta\gamma_{\max}}{2} + S\Delta\varepsilon_n \quad . \tag{22}$$

For fatigue life prediction, this formulation is expressed as follows:

$$\frac{\Delta\gamma_{\max}}{2} + S\Delta\varepsilon_n = [(1+\nu) + S(1-\nu)]\frac{\sigma'_f}{E}(2N_f)^b + [1.5 + 0.5S]\varepsilon'_f(2N_f)^c, \tag{23}$$

where,

$$S = \frac{\frac{\tau'_{\mathrm{f}}}{\mathrm{G}}(2\mathrm{N_f})^{b_\gamma} + \gamma'_{\mathrm{f}}(2\mathrm{N_f})^{c_\gamma} - (1+\nu)\frac{\sigma'_f}{E}(2\mathrm{N_f})^b - 1.5\varepsilon'_f(2\mathrm{N_f})^c}{(1-\nu)\frac{\sigma'_f}{E}(2\mathrm{N_f})^b + 0.5\varepsilon'_f(2\mathrm{N_f})^c}. \tag{24}$$

Based on the work of Brown and Miller [39], Fatemi and Socie [40] concluded that tensile normal stress in the maximum shear stress plane accelerates crack growth by separating the crack surfaces and consequently reducing frictional forces. The following damage model may be interpreted as the cyclic shear strain modified by the normal stress to include the crack closure effects described:

$$\frac{\Delta\gamma_{\max}}{2}\left(1 + \kappa\frac{\sigma_{\mathrm{n,max}}}{\sigma'_{yield}}\right) = \frac{\tau'_f}{G}\left(2N_f\right)^{b_\gamma} + \gamma'_f\left(2N_f\right)^{c_\gamma}, \tag{25}$$

where $\frac{\Delta\gamma_{\max}}{2}$ is the maximum shear strain amplitude and $\sigma_{\mathrm{n,max}}$ is the maximum normal stress on the plane where $\frac{\Delta\gamma_{\max}}{2}$ occurs. The material parameter κ represents the influence of the normal stress, $\sigma_{\mathrm{n,max}}$. In addition, σ'_{yield} represents the cyclic yield strength of the material and is included to make the maximum normal stress component dimensionless and proportional to the shear strain.

The material parameter κ is expressed in the following way:

$$\kappa = \left[\frac{\frac{\tau'_{\mathrm{f}}}{\mathrm{G}}(2\mathrm{N_f})^{b_\gamma} + \gamma'_{\mathrm{f}}(2\mathrm{N_f})^{c_\gamma}}{(1+\nu)\frac{\sigma'_f}{E}(2\mathrm{N_f})^b + 1.5\varepsilon'_f(2\mathrm{N_f})^c} - 1\right]\frac{\sigma_{\mathrm{yield}}}{\sigma'_f(2\mathrm{N_f})^b}. \tag{26}$$

3.3. Energy-based criteria

Energy based criteria are generally classified into three different groups, depending on the kind of strain energy density per cycle assumed as the damage parameter. In the first group, elastic strain energy is considered as the damage parameter, and the criteria are used for high cycle fatigue regimes. Secondly, for low cycle fatigue regimes, plastic strain energy is considered as the damage parameter. The last group is based on a combination of elastic and plastic strain energies for both high and low cycle fatigue regimes. The first of the energy-based damage parameter considered was proposed by Smith et al [43], SWT, for predicting fatigue life under uniaxial tension-compression conditions. The parameter was originally defined as:

$$\sigma_{\mathrm{n,max}}\frac{\Delta\varepsilon}{2} = \frac{\sigma'^2_{\mathrm{f}}}{E}(2\mathrm{N_f})^{2b} + \sigma'_{\mathrm{f}}\varepsilon'_{\mathrm{f}}(2\mathrm{N_f})^{b+c}, \tag{27}$$

This parameter was modified for proportional and non-proportional multiaxial loading conditions of materials that fail predominantly by crack growth on planes of maximum tensile strain or stress, i.e. by Mode I. In these materials, cracks nucleate in shear, but early life is controlled by crack growth on planes perpendicular to the maximum principal stress and strain. Socie [44] proposed a modification to the

SWT parameter in order to take into account only stresses and strains occurring in the critical plane. This became the most well-known form of the parameter and is mathematically represented by:

$$\sigma_{\mathrm{n,max}}\frac{\Delta\varepsilon_1}{2}=\frac{\sigma_{\mathrm{f}}'^2}{\mathrm{E}}(2\mathrm{N_f})^{2b}+\sigma_{\mathrm{f}}'\varepsilon_{\mathrm{f}}'(2\mathrm{N_f})^{b+c}. \tag{28}$$

where $\frac{\Delta\varepsilon_1}{2}$ represents the maximum normal strain, and accordingly $\sigma_{\mathrm{n,max}}$ is calculated on the plane where $\frac{\Delta\varepsilon_1}{2}$ occurs.

Liu [45] proposed a criterion based on the virtual strain energy concept. He used two different formulations depending on the failure mode, one for tensile failure, ΔW_I, and another one for shear failure, ΔW_{II}. The first criterion, ΔW_I, considers the axial work, $\Delta\sigma\Delta\varepsilon$, as the main damage parameter, and assumes as the critical plane the plane in which this parameter reaches its maximum value. On the other hand, for the second criterion, ΔW_{II}, the critical plane is the one that maximises the shear work, $\Delta\tau\Delta\gamma$:

$$\Delta W_I=(\Delta\sigma\Delta\varepsilon)_{max}+(\Delta\tau\Delta\gamma) \quad , \tag{29}$$

and,

$$\Delta W_{II}=(\Delta\sigma\Delta\varepsilon)+(\Delta\tau\Delta\gamma)_{max} \quad . \tag{30}$$

For fatigue life prediction, these formulations are expressed as:

$$\Delta W_I=4\sigma_f'\varepsilon_f'\left(2N_f\right)^{b+c}+\frac{4\sigma_f'^2}{E}\left(2N_f\right)^{2b} \quad , \tag{31}$$

and,

$$\Delta W_{II}=4\tau_f'\gamma_f'\left(2N_f\right)^{b_\gamma+c_\gamma}+\frac{4\tau_f'^2}{G}\left(2N_f\right)^{2b_\gamma} \quad . \tag{32}$$

Finally, two formulations were proposed by Ince-Glinka [46], based on search for specific planes experiencing the maximum amount of a generalised strain energy (GSE). The GSE damage parameter includes both the normal and shear strain energy terms:

$$W_{gen}^{*}=\left(\tau_{\max}\frac{\Delta\gamma^e}{2}+\frac{\Delta\tau}{2}\frac{\Delta\gamma^p}{2}+\sigma_{\mathrm{n,max}}\frac{\Delta\varepsilon_{\mathrm{n}}^e}{2}+\frac{\Delta\sigma_{\mathrm{n}}}{2}\frac{\varepsilon_{\mathrm{n}}^p}{2}\right)_{\max} \quad . \tag{33}$$

200 This formulation takes into account the effects of mean stress and non-proportional hardening through the elastic shear and normal strain energy terms by including the maximum shear stress, $\tau_{\max}$, and the maximum normal stress, $\sigma_{\max}$, in the formulation of the damage parameter. In addition, the shear strain energy terms reflect the initiation and growth of cracks, and the normal strain energy terms accelerate the crack growth.

The shear strain energy terms in Eq. 33 can be normalised with the shear stress amplitude, $\frac{\Delta\tau}{2}$ and the normal strain energy terms can be normalised with the normal stress amplitude, $\frac{\Delta\sigma}{2}$ to transform the generalized strain energy parameter to the form of generalized strain amplitude (GSA):

$$\frac{\Delta\varepsilon_{gen}^{*}}{2}=\left(\frac{\tau_{\max}}{\Delta\tau/2}\frac{\Delta\gamma^e}{2}+\frac{\Delta\gamma^p}{2}+\frac{\sigma_{\mathrm{n,max}}}{\Delta\sigma_{\mathrm{n}}/2}\frac{\Delta\varepsilon_{\mathrm{n}}^e}{2}+\frac{\varepsilon_{\mathrm{n}}^p}{2}\right)_{\max} \quad . \tag{34}$$

Based on Basquin's relationship presented in Eqs. 11 and 12, and assuming a fatigue life of one cycle, i.e. $2N_f=1$, the shear and normal stress amplitudes become:

$$\frac{\Delta\sigma}{2}=\sigma_f'(2N_f)^b=\sigma_f' \quad , \tag{35}$$

and,

$$\frac{\Delta\tau}{2}=\tau_f'(2N_f)^{b_\gamma}=\tau_f' \quad . \tag{36}$$

Substituting Eqs. 35 and 36 into Eq. 34, the multiaxial fatigue damage parameter based on the generalized strain amplitude becomes:

$$\frac{\Delta\varepsilon_{gen}^{*}}{2}=\left(\frac{\tau_{\max}}{\tau_f'}\frac{\Delta\gamma^e}{2}+\frac{\Delta\gamma^p}{2}+\frac{\sigma_{\mathrm{n,max}}}{\sigma_f'}\frac{\Delta\varepsilon_{\mathrm{n}}^e}{2}+\frac{\varepsilon_{\mathrm{n}}^p}{2}\right)_{\max} \quad . \tag{37}$$

4. Results

This section presents the general behaviour and fatigue life prediction obtained with each of the strain- and energy-based formulations presented in the previous section.

4.1. Critical Plane Search

For a loaded specimen, stress and strain magnitudes at a given point vary depending on the orientation of a plane passing through that point. In this work, stress and strain components on arbitrary planes are calculated using a coordinate transformation matrix with respect to plane orientation. The coordinate system, $x-y-z$, on the surface of the cruciform specimen is shown in Fig. 2. The planes of interest are obtained by first rotating the coordinate system by an angle θ about the x axis (Eq. 38) and then by an angle ϕ about the z axis (Eq. 39). The rotation matrix for rotations about x and z are given respectively as:

$$a_\theta = \begin{vmatrix} 1 & 0 & 0 \\ 0 & \cos\theta & \sin\theta \\ 0 & -\sin\theta & \cos\theta \end{vmatrix} \quad , \tag{38}$$

$$a_\phi = \begin{vmatrix} \cos\phi & \sin\phi & 0 \\ -\sin\phi & \cos\phi & 0 \\ 0 & 0 & 1 \end{vmatrix} \quad . \tag{39}$$

Finally, the general transformation matrix for rotations about x axis first and then z axis is defined as:

$$a_{\theta\phi} = a_\theta a_\phi = \begin{vmatrix} \cos\theta & \sin\theta\cos\phi & \sin\theta\sin\phi \\ -\sin\theta & \cos\theta\cos\phi & \cos\theta\sin\phi \\ 0 & -\sin\phi & \cos\phi \end{vmatrix} \quad . \tag{40}$$

Consequently, the stresses on specific planes can be calculated by:

$$\sigma'_{ij} = a_{\theta\phi}\sigma_{ij}a^{\intercal}_{\theta\phi} \quad , \tag{41}$$

where $a^{\intercal}_{\theta\phi}$ defines the transpose of the general transformation matrix presented in Eq. 40. As is presented above, the elastic and plastic components of strain correspondent to σ'_{ij} are calculated according to Eq. 6. The general variation of normal and shear stresses for the equi-biaxial case (CX03) with respect to θ and ϕ are presented in Figs. 8 and 9. Similarly, Figs. 10 to 15 present the variation of each of the strain- and energy-based parameters presented in the previous section with respect to θ and ϕ.

Analysing Figs. 10–15, the most noticeable difference between strain- and energy-based parameters is that strain-based parameters tend to have more pronounced peaks, while energy-based parameter parameters have spread out maximums. Wang-Brown and Fatemi-Socie parameters present similar variation as a function of θ and ϕ. That is expected, as both parameters (Eq. 23 and 25) consider the planes of maximum shear strain amplitude, $\frac{\Delta\gamma}{2}$, as critical planes. The difference between the two strain-based formulations (WB and FS) consists basically in the minimum values obtained with each of them.

For the energy-based formulations, only the SWT and Liu parameters present a symmetrical variation. The SWT parameter is always searching for the plane which maximises the normal work. Therefore, its maximum peaks repeat every 90 degrees, similar to WB and FS parameters. In the case of Liu's formulation, Fig. 13 illustrates the sum of normal and shear virtual works and not Liu I or Liu II in particular. That is exactly why the variations of GSE and GSA are not symmetrical (Figs. 14 and 15). For GSE and GSA critical planes are the planes which maximise the parameter as a whole, not just the maximum shear or normal strain energy density.

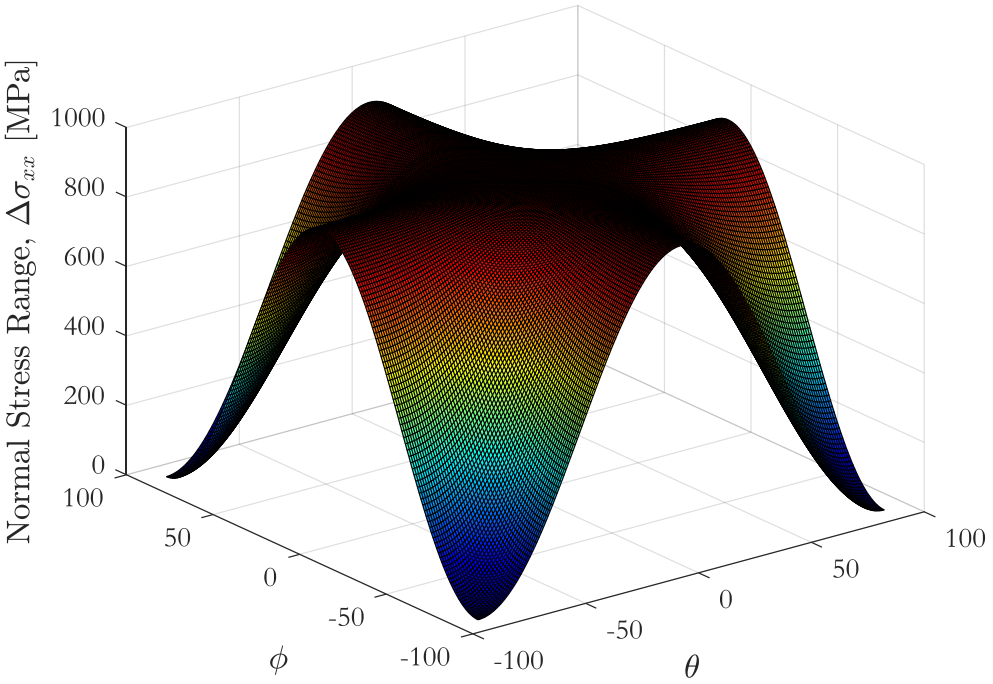

Figure 8: Variation of normal stress with respect to θ and ϕ. Equi-biaxial condition.

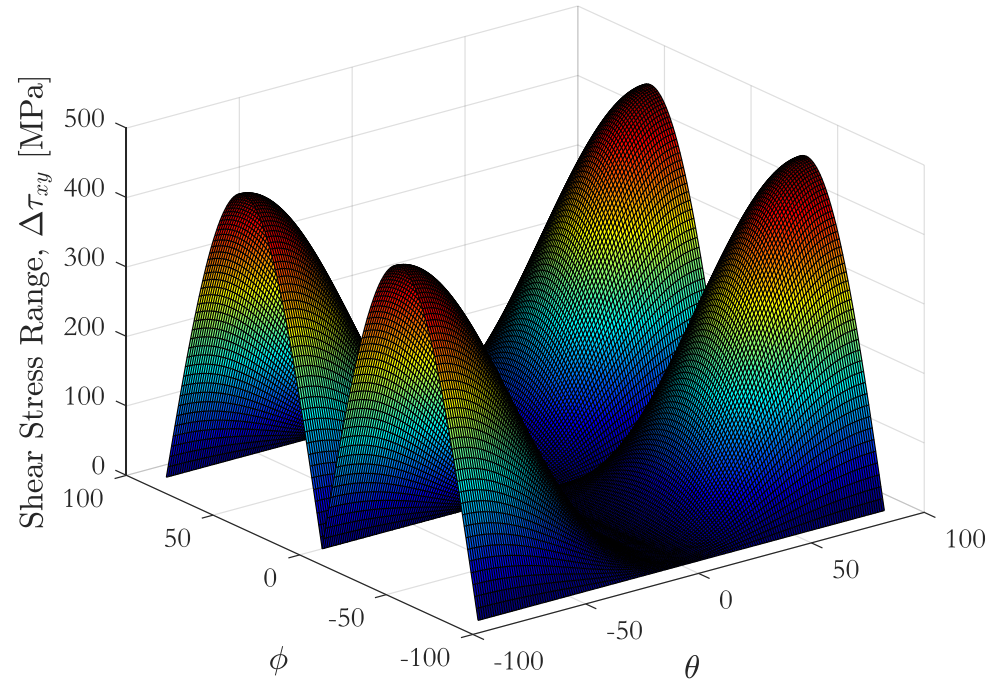

Figure 9: Variation of shear stress with respect to θ and ϕ. Equi-biaxial condition.

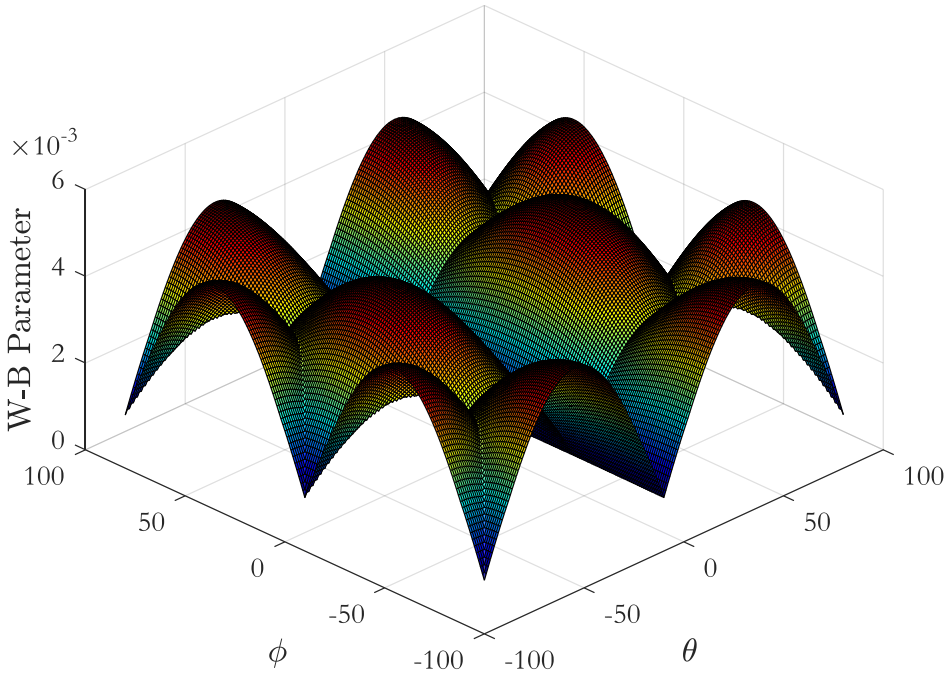

Figure 10: Wang-Brown parameter. Variation with respect to θ and ϕ. Equi-biaxial condition.

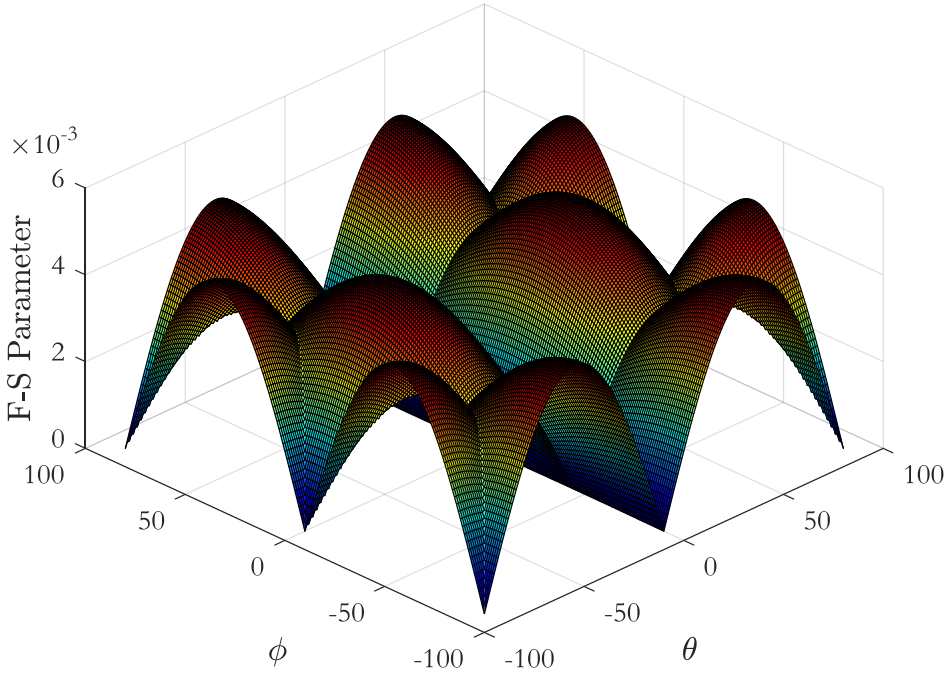

Figure 11: Fatemi-Socie parameter. Variation with respect to θ and ϕ. Equi-biaxial condition.

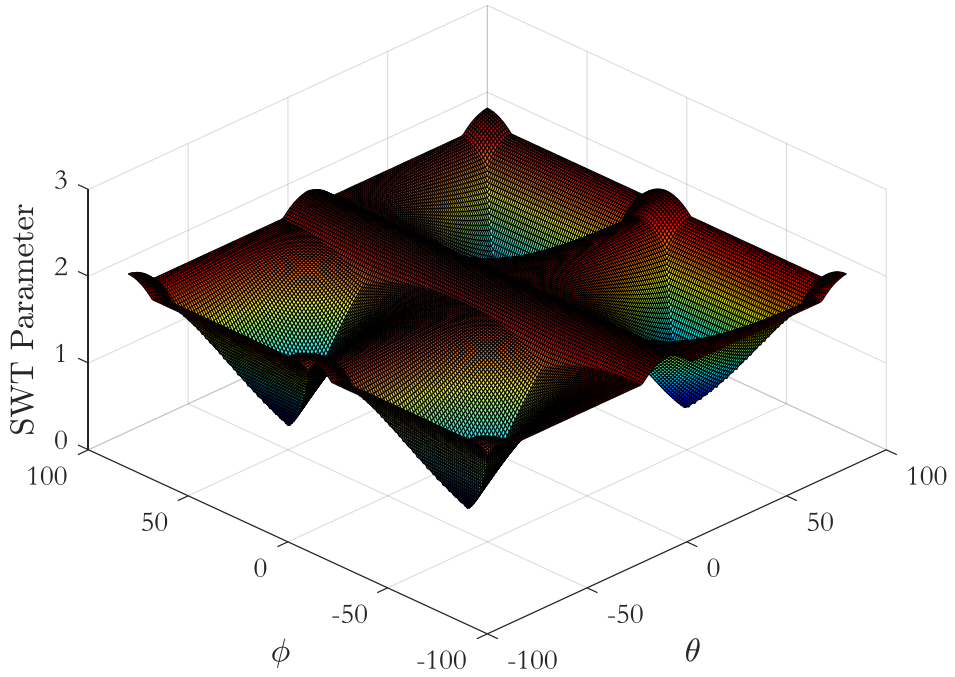

Figure 12: Smith-Watson-Topper parameter. Variation with respect to θ and ϕ. Equi-biaxial condition.

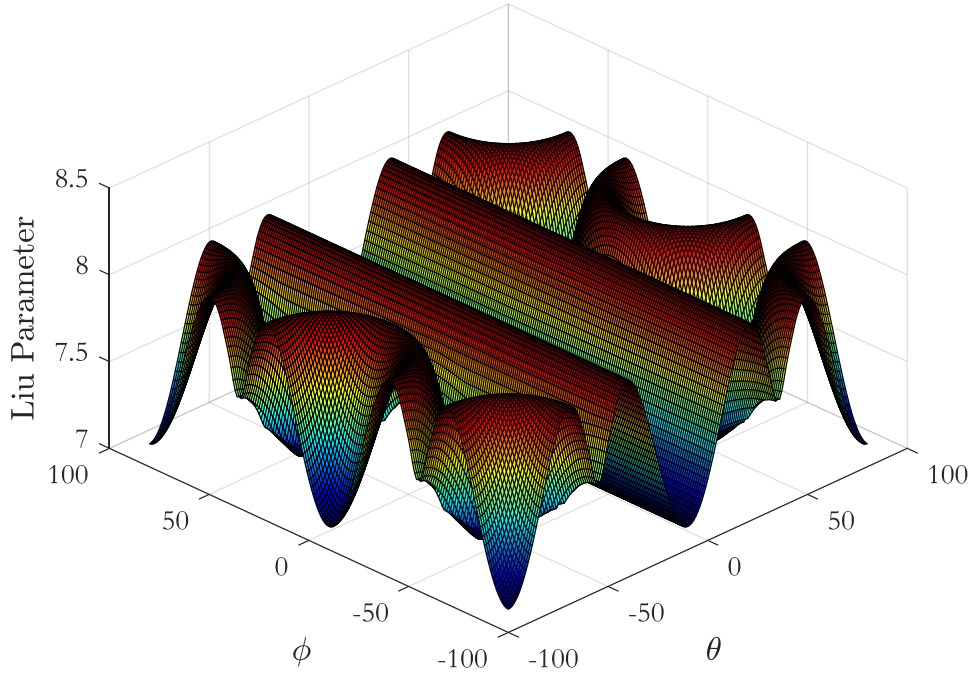

Figure 13: Liu parameter. Variation with respect to θ and ϕ. Equi-biaxial condition.

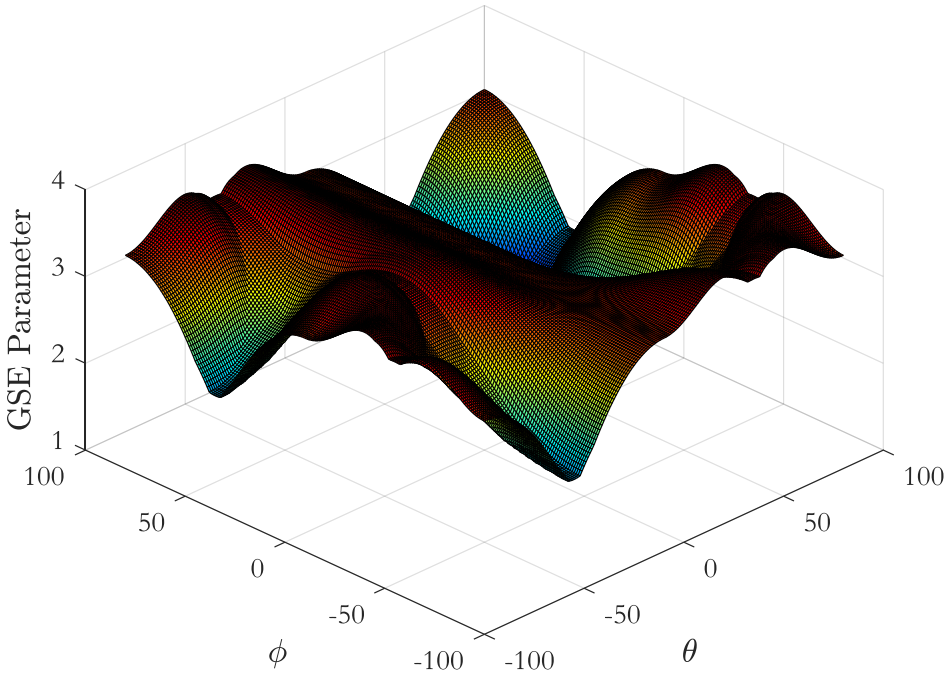

Figure 14: GSE parameter. Variation with respect to θ and ϕ. Equi-biaxial condition.

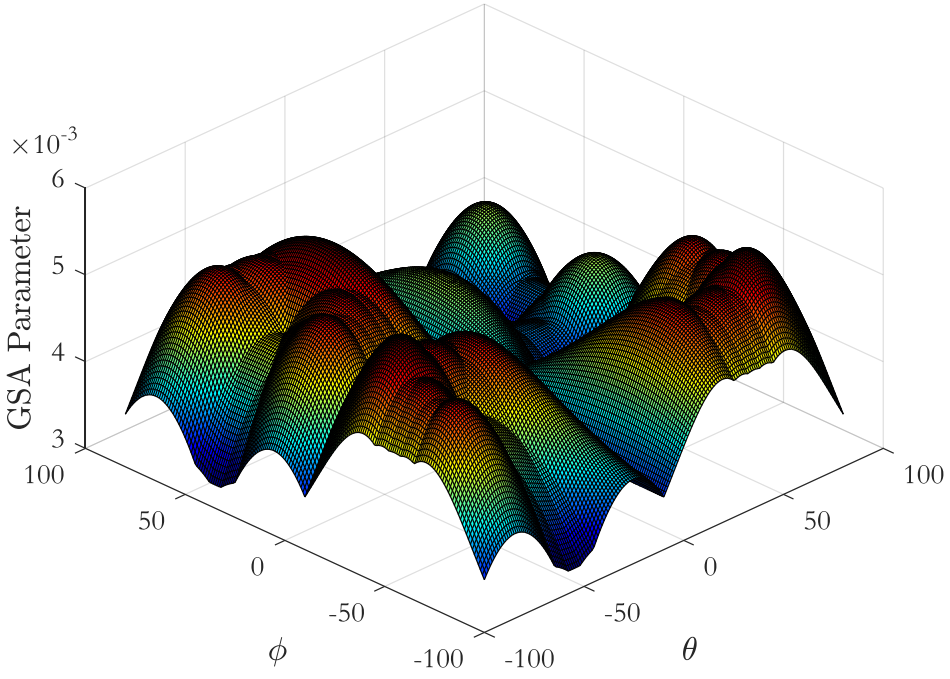

Figure 15: GSA parameter. Variation with respect to θ and ϕ. Equi-biaxial condition.

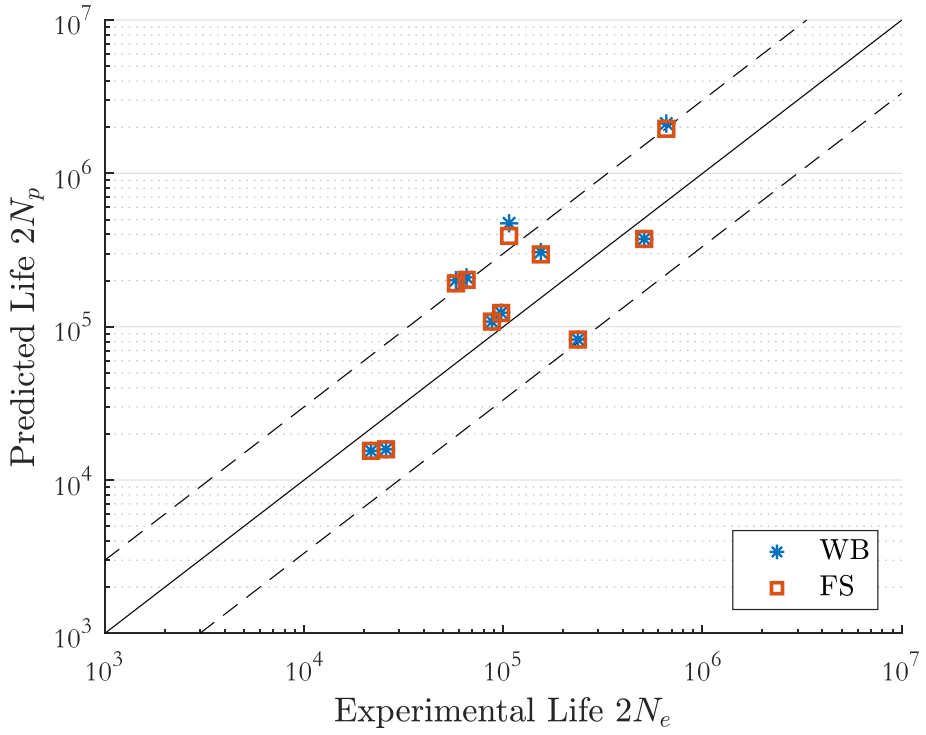

Figure 16: Strain-based parameters. Fatigue life prediction.

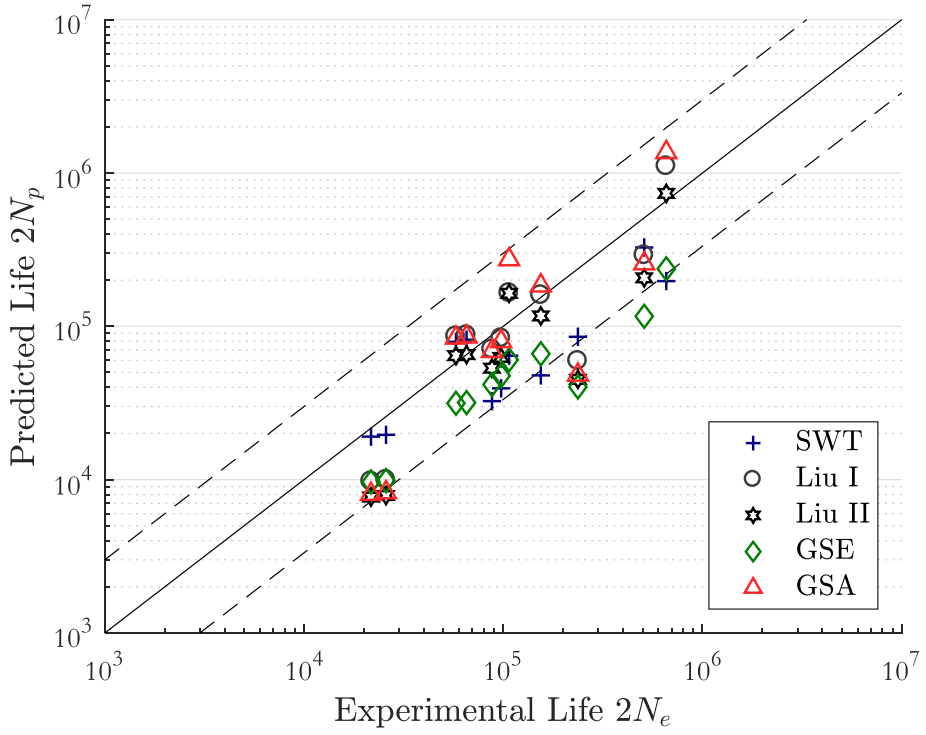

Figure 17: Energy-based parameters. Fatigue life prediction.

4.2. Fatigue Life Prediction

After calibrating all the models using material parameters and results available in the literature [33, 40, 46], their performance was assessed using the biaxial test data presented in Tab. 1. Fatigue lives were calculated using the formulations presented in Eqs. 17 to 37, considering the value of each damage parameter on the material plane where they reached their maximum. The results are plotted against the experimental fatigue lives in Fig. 16 for strain-based approaches, and Fig. 17 for energy-based approaches. Figure 18 summarize the overall result. The solid black line in the plot represents perfect correlation between predicted ($2N_p$) and experimental life ($2N_e$). In contrast, predictions lying above this line represent non-conservative predictions, and data points below the line represents conservative predictions. Further, the dashed lines represent the factor of three scatter bands.

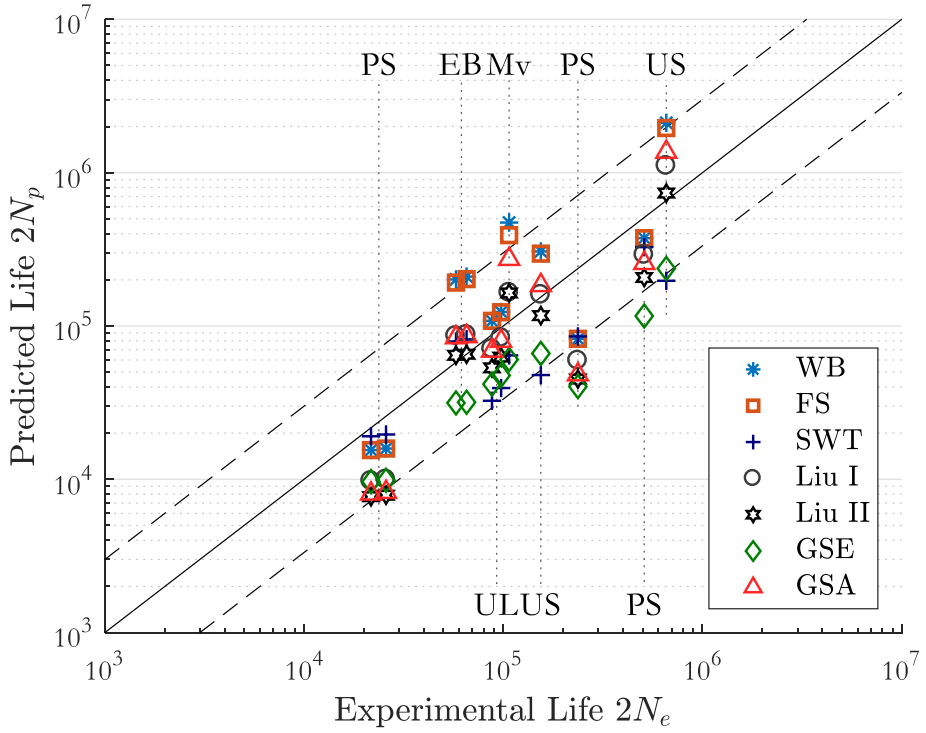

Figure 18: Fatigue life prediction with strain and energy-based formulations.

5. Discussion

Considering Fig. 16, which presents the fatigue life prediction for the strain-based parameters by Fatemi-Socie (FS) and Wang-Brown (WB), it is observed that both parameters present similar predictions (an expected result as both parameters present similar variations in Figs. 10 and 11). These two criteria show their best predictions for the pure shear condition (CX05 and CX11), uniaxial load (CX01 and CX04) and uniaxial stress (CX07). Despite the good agreement with the pure shear loading case (CX06), this result is misleading as this was a runout specimen. Their worst predictions are for the equi-biaxial case (CX02 and CX03), minimum von Mises (CX08), uniaxial equivalent with lower strain range (CX09) and pure shear with lower stress range (CX10). Nevertheless, both strain-based parameters present good correlation, with almost all their predictions within the factor of three scatter bands.

Considering Fig. 17 and the energy-based criteria, best predictions are obtained with the SWT and Liu parameters. Almost all predictions obtained with SWT and Liu lie within the factor of three scatter bands. Comparing the two of them, the SWT parameter gives more conservative predictions, which is a desirable characteristic for the safe design of complex engineering components. On the other hand, better agreement with the experimental data is obtained with Liu, despite conservative predictions for the pure shear cases. Good correlation is also obtained with the GSE and GSA parameters. However, despite the higher scatter, the GSA is in better correlation with the experimental data, as some of the predictions obtained with the GSE parameter are over-conservative.

In an attempt to characterise the fatigue behaviour of Waspaloy under both proportional (in-phase) and non-proportional (out-of-phase) loading at room temperature and elevated temperature, Pattison [21] used a hyperbolic co-tangent to correlate numerous stress-, strain and energy-based parameters to initiation life. The objective of their research was the assessment of how alternative multiaxial damage parameters perform as direct replacements to Walker Strain parameter. Similar to the conclusions presented here, Pattison pointed out that the Liu parameter performed the best in collapsing the fatigue data points to the initiation life curve. However, they note that this parameter is not ideal, since there is no explicit mean stress correction term.

6. Conclusion

Further investigation of the biaxial fatigue behaviour of Waspaloy has concluded that all the strain- and energy-based formulations assessed give reasonably good correlation for most of the loading cases. In particular, better agreement with experimental data has been obtained with the SWT and Liu II parameter. The Liu II parameter gives particularly good predictions for the low cycle fatigue regime ($< 10^5$ cycles), with slightly higher error for the minimum von Mises loading case. However, for high cycle fatigue, Liu II gives predictions with significant scatter in results. In contrast, the SWT does not present as close agreement with the experimental data as the Liu II parameter, but all the predictions obtained with the SWT parameter lie on the conservative side of the plot.

Therefore, for the safe design of complex engineering components made of Waspaloy that operate in the low cycle fatigue regime, and in loading conditions similar to those shown in this work, the Liu II parameter is recommended. For high cycle fatigue, or more conservative designs the SWT parameter is recommended.

Acknowledgements

The authors are grateful for the support of Rolls-Royce plc and the Brazilian National Council of Technological and Scientific Development (CNPq), grant number 207297/2015-0. A portion of this work was part of a Collaborative R&T Project SILOET supported by the Technology Strategy Board.

References

[1] J. Castro, M. Meggiolaro, Fatigue design techniques (in 3 volumes), CreateSpace, Scotts Valley, CA, USA.
[2] R. I. Stephens, A. Fatemi, R. R. Stephens, H. O. Fuchs, Metal fatigue in engineering, John Wiley & Sons, 2000.
[3] J. Sahadi, R. Paynter, D. Nowell, S. Pattison, N. Fox, Comparison of multiaxial fatigue parameters using biaxial tests of waspaloy, International Journal of Fatigue 100 (2017) 477–488.
[4] G. Lanza, Strength of shafting subjected to both twisting and bending, Trans ASME 8 (1886) 121–196.
[5] W. Mason, Alternating stress experiments, Proceedings of the Institution of Mechanical Engineers 92 (1) (1917) 121–196.
[6] W. Mason, The distribution of stress in round mild steel bars under alternating torsion or bending, Reports British Association for the Advancement of Science, London (1923) 386–409.
[7] Y. Garud, Multiaxial fatigue: a survey of the state of the art, Journal of Testing and Evaluation 9 (3) (1981) 165–178.
[8] W. Mason, W. Delaney, Alternating combined stress experiments, Reports British Association for the Advancement of Science, London (1921) 329–341.
[9] H. Gough, H. Pollard, The strength of metals under combined alternating stresses, Proceedings of the institution of mechanical engineers 131 (1) (1935) 3–103.
[10] H. Gough, Engineering steels under combined cyclic and static stresses, Proceedings of the Institution of Mechanical Engineers 160 (1) (1949) 417–440.
[11] T. Nisihara, M. Kawamoto, The strength of metals under combined alternating bending and torsion, Trans. Japan Soc. Mech. Engrs 7 (1941) 185–194.
[12] T. Nishihara, M. Kawamoto, A new criterion for the strength of metals under combined alternating stresses, Memoirs of College of Engineering, Kyoto Imperial University 11 (1944) 65–83.
[13] T. Nishihara, M. Kawamoto, The strength of metals under combined alternating bending and torsion with phase difference, Memoirs of the College of Engineering, Kyoto Imperial University 11 (5) (1945) 85–112.
[14] V. Bonnand, J. Chaboche, P. Gomez, P. Kanouté, D. Pacou, Investigation of multiaxial fatigue in the context of turboengine disc applications, International Journal of Fatigue 33 (8) (2011) 1006–1016.
[15] S. Kalluri, P. J. Bonacuse, In-phase and out-of-phase axial-torsional fatigue behavior of haynes 188 superalloy at 760 c, in: Advances in multiaxial fatigue, ASTM International, 1993.
[16] M. S. Found, U. S. Fernando, K. J. Miller, Requirements of a new multiaxial fatigue testing facility, in: Multiaxial fatigue, ASTM International, 1985.
[17] J. Andrews, E. Ellison, A testing rig for cycling at high biaxial strains, Journal of Strain Analysis 8 (3) (1973) 168–175.
[18] A. Makinde, L. Thibodeau, K. Neale, Development of an apparatus for biaxial testing using cruciform specimens, Experimental mechanics 32 (2) (1992) 138–144.
[19] J. Boehler, S. Demmerle, S. Koss, A new direct biaxial testing machine for anisotropic materials, Experimental mechanics 34 (1) (1994) 1–9.

[20] A. Hannon, P. Tiernan, A review of planar biaxial tensile test systems for sheet metal, Journal of materials processing technology 198 (1) (2008) 1–13.
[21] S. J. Pattison, Multi-axial and thermo-mechanical loading effects in nickel-based disc superalloys / Stephen John Pattison., 2012.
[22] Al Bin Mousa, Jafar, Multiaxial fatigue characterization and modeling of az31b magnesium extrusion, Ph.D. thesis (2012).
URL http://hdl.handle.net/10012/6431
[23] A. Ince, G. Glinka, A. Buczynski, Computational modeling of multiaxial elasto-plastic stress–strain response for notched components under non-proportional loading, International Journal of Fatigue 62 (2014) 42–52.
[24] B.-R. You, S.-B. Lee, A critical review on multiaxial fatigue assessments of metals, International Journal of Fatigue 18 (4) (1996) 235–244.
[25] E. Macha, C. Sonsino, Energy criteria of multiaxial fatigue failure, Fatigue and Fracture of Engineering Materials and Structures 22 (12) (1999) 1053–1070.
[26] A. Carpinteri, A. Spagnoli, S. Vantadori, A review of multiaxial fatigue criteria for random variable amplitude loads, Fatigue & Fracture of Engineering Materials & Structures 40 (7) (2017) 1007–1036.
[27] A. Fatemi, N. Shamsaei, Multiaxial fatigue: An overview and some approximation models for life estimation, International Journal of Fatigue 33 (8) (2011) 948–958.
[28] D. Socie, G. Marquis, Multiaxial fatigue, Warrendale, PA: Society of Automotive Engineers, 1999. 502.
[29] I. V. Papadopoulos, P. Davoli, C. Gorla, M. Filippini, A. Bernasconi, A comparative study of multiaxial high-cycle fatigue criteria for metals, International Journal of Fatigue 19 (3) (1997) 219–235.
[30] Y.-Y. Wang, W.-X. Yao, Evaluation and comparison of several multiaxial fatigue criteria, International Journal of Fatigue 26 (1) (2004) 17–25.
[31] A. Carpinteri, A. Spagnoli, S. Vantadori, D. Viappiani, A multiaxial criterion for notch high-cycle fatigue using a critical-point method, Engineering Fracture Mechanics 75 (7) (2008) 1864–1874.
[32] L. Reis, B. Li, M. De Freitas, Crack initiation and growth path under multiaxial fatigue loading in structural steels, International Journal of Fatigue 31 (11) (2009) 1660–1668.
[33] P. Lopez-Crespo, B. Moreno, A. Lopez-Moreno, J. Zapatero, Study of crack orientation and fatigue life prediction in biaxial fatigue with critical plane models, Engineering Fracture Mechanics 136 (2015) 115–130.
[34] B. Weber, A. Carmet, J. Clément, J. Robert, Les criteres de fatigue multiaxiaux et leur application au dimensionnement en fatigue des structures, in: Société Française de Métallurgie et de Matériaux. Journées de printemps, 1999, pp. 29–1.
[35] B. Crossland, Effect of large hydrostatic pressures on the torsional fatigue strength of an alloy steel, in: Proc. Int. Conf. on Fatigue of Metals, Vol. 138, Institution of Mechanical Engineers London, 1956.
[36] W. N. Findley, A theory for the effect of mean stress on fatigue of metals under combined torsion and axial load or bending, no. 6, Engineering Materials Research Laboratory, Division of Engineering, Brown University, 1958.
[37] T. Matake, An explanation on fatigue limit under combined stress, Bulletin of JSME 20 (141) (1977) 257–263.
[38] K. Walker, The effect of stress ratio during crack propagation and fatigue for 2024-t3 and 7075-t6 aluminum, in: Effects of environment and complex load history on fatigue life, ASTM International, 1970.
[39] M. Brown, K. Miller, A theory for fatigue failure under multiaxial stress-strain conditions, Proceedings of the Institution of Mechanical Engineers 187 (1) (1973) 745–755.
[40] A. Fatemi, P. Kurath, Multiaxial fatigue life predictions under the influence of mean-stresses, Journal of Engineering Materials and Technology 110 (4) (1988) 380–388.
[41] C. Wang, M. Brown, Life prediction techniques for variable amplitude multiaxial fatiguepart 2: comparison with experimental results, Journal of engineering materials and technology 118 (3) (1996) 371–374.
[42] F. Kandil, M. Brown, K. Miller, Biaxial low-cycle fatigue failure of 316 stainless steel at elevated temperatures, in: Mechanical behaviour and nuclear applications of stainless steel at elevated temperatures, 1982.
[43] K. Smith, T. Topper, P. Watson, A stress-strain function for the fatigue of metals(stress-strain function for metal fatigue including mean stress effect), Journal of materials 5 (1970) 767–778.
[44] D. Socie, Multiaxial fatigue damage models, Journal of Engineering Materials and Technology 109 (4) (1987) 293–298.
[45] K. Liu, A method based on virtual strain-energy parameters for multiaxial fatigue life prediction, in: Advances in multiaxial fatigue, ASTM International, 1993.
[46] A. Ince, G. Glinka, A generalized fatigue damage parameter for multiaxial fatigue life prediction under proportional and non-proportional loadings, International Journal of Fatigue 62 (2014) 34–41.